Archive of Applied Mechanics 71 (2001) 182 – 192 © Springer-Verlag 2001

Modelling of functionally graded materials by numerical homogenization

S. Schmauder, U. Weber

Summary In this contribution, the mechanical behaviour of different ZrO_2/NiCr 80 20 compositions is analysed and compared with experimental findings. The microwave-sintered material is found to possess a slightly dominant ceramic matrix for intermediate volume fractions. Its thermal expansion coefficient deviates from the rule of mixture. The modulus and the stress strain behaviour can be simulated by a numerical homogenization procedure, and the influence of residual stresses is found to be negligible. A newly introduced parameter (matricity) describes the mutual circumvention of the phases and is found to strongly control the stress level of the composite, globally as well as locally. Finally, a graded component and a metal/ceramic bi-material are compared for thermal as well as mechanical loading.

Key words finite element method, interpenetrating microstructures, matricity, residual stress, homogenization

1 Introduction

Functionally graded materials (FGMs) are difficult to simulate because of the lacking material data for different compositions at different locations. The main reason for this situation is the nonlinear dependence of the elastic-plastic properties on the phase composition of composites. Therefore, a great deal of work has been performed recently to overcome this problem and to estimate the properties of composites.

The following examples are chosen to demonstrate some recent achievements in this respect. In [1], a micromechanical model is applied to study random and discrete microstructures and their interrelations with residual stresses; crystal plasticity effects are taken into account in differently graded FGMs with a layer structure. This model is compared with continuous models, and their equivalence is demonstrated with respect to macroscopic behaviour while strong local stress and strain concentrations are found. The analysis of the influence of thermal stresses and failed particles on macroscopic stress-strain curves, based on a constitutive Eshelby-type solution is restricted to dilute particle-reinforced materials, [2]. Calculations of the thermo-elastic response in C/SiC composite systems showed that effective moduli, expansion coefficients and heat conductivities do not require detailed micromechanical analyses, but rather can be derived from homogenization models or, in the case of interpenetrating microstructures, from self-consistent estimates, [3]. Nonlinear effects have not been taken into account in this study. The influence of thermal residual stresses on the coefficient of thermal expansion for metal-matrix, ceramic-matrix and interpenetrating Al/SiC composites, taking temperature dependent material properties – especially of Al – into account, are given in [4] using unit cell-type FE-models. They were compared with upper and lower analytical bounds of composites with homogeneous phase distributions. Some FE-analysis of macroscopic and

Received 23 November 1999; accepted for publication 26 May 2000

S. Schmauder (✉), U. Weber
Staatliche Materialprüfungsanstalt (MPA) University of Stuttgart,
Pfaffenwaldring 32, D-70569 Stuttgart, Germany
e-mail: siegfried.schmauder@mpa.uni-stuttgart.de
Fax: (0711)685 2635

Financial support by the German Research Society (DFG) under grant Schm 746/12-1,2 is gratefully acknowledged. We would also like to thank Prof. Willert-Porada of the Bayreuth University for the experimental results.

microscopic elasto-plastic deformation due to thermal and mechanical axial and bending loading of layered Ni/Al_2O_3 composites with graded interfaces based on a single unit cell-type model with hexagonal or square packing and with mesomechanical cells of the random-arrangement type (taking hundreds of hexagonal grains into account) has been performed in [5]. FE-models have been also applied in [6] for the same Ni/Al_2O_3 composite with and without graded interfaces, for different specimen geometries, demonstrating the reduction in maximum residual stresses except for the shear stresses at interface edges by gradation.

However, a major drawback of most literature examples is the lack of experimental comparison for the calculated thermal-mechanical properties. Moreover, these numerical and analytical-numerical models are rather complicated, and typically restricted to two dimensions. In the following, another more promising procedure is described.

Recently, a systematic study has been successfully performed on the strengthening effects of inclusion-type 2D and 3D microstructures, [7–10]. In this paper, thermo-elastic-plastic properties of ZrO_2/NiCr 80 20 composites and FGMs are predicted, based on a new numerical homogenization technique, [11–17], and results will be compared to experiments.

Composites consisting of phases with strongly different properties have the potential to be applied in new application fields as they comprise otherwise incompatible properties. While the deformation behaviour of inclusion-type microstructures has been successfully modelled in the past for brittle fiber or particulate reinforced metal matrix composites, [7, 8], this was not achieved until recently in the case of interpenetrating microstructures where both phases are connected throughout the material. Such microstructures are typically observed in the composition range of 30–70%, while inclusion-type microstructures are typical for dilute systems with phase volume fractions between 0–30%. Specifically, FGMs can depict the full composition range in material transitions. As processing techniques are nowadays available to design material transitions from inclusion to interpenetrating type of microstructures, experience in modelling of the full composition range is still lacking. This paper is intended to bridge this gap in the case of ZrO_2/NiCr 80 20 composites where the full compositional range is available from a powder-metallurgical route, [18], such that comparison in properties and predictions can be made.

2
Models

Three models are used for the simulation of the elastic properties of ZrO_2/NiCr 80 20 composites with phases α = ZrO_2 (E = 46 GPa, μ = 0.29, α = 10.3E-06 l/K) and β = NiCr 80 20 (E = 121 GPa, μ = 0.29, α = 17.3E-06 l/K) in this paper, while the thermo-elastic-plastic behaviour will be analysed numerically. The microstructure of a ZrO_2/NiCr 80 20 composite with a volume fraction of ceramic f_{ZrO_2} = 30% is shown in Fig. 1. In the case of an inclusion-type microstructure, the self-consistent embedded cell model is applied which is described in

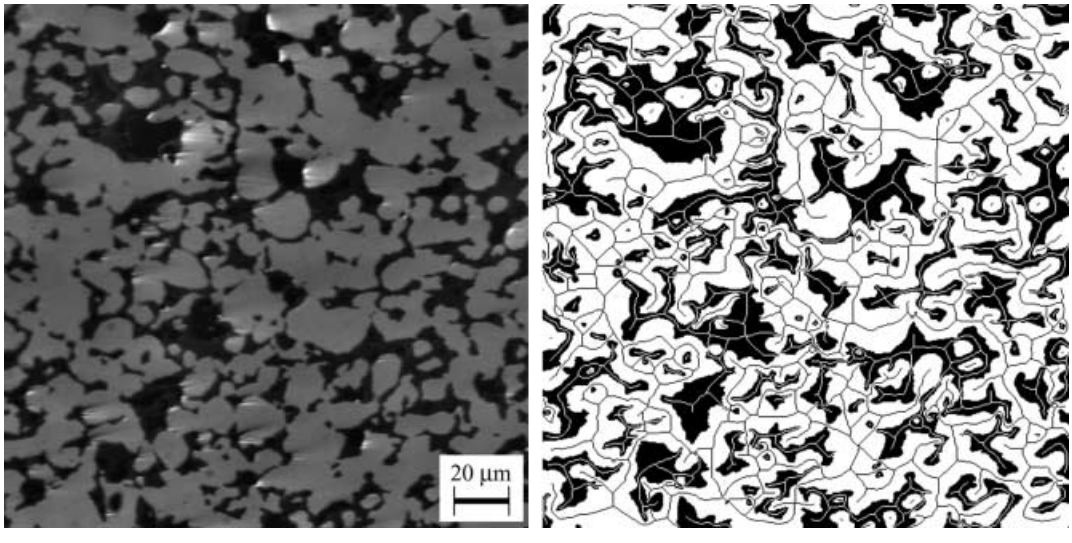

Fig. 1. Micrograph of ZrO_2/NiCr 80 20 with 30% volume fraction of ceramic. Left side: greyscale picture (grey = NiCr 80 20, dark = ZrO_2, black = porosity), right side: binary image with skeleton lines

[7–10, 19]. The embedded cell model is a special numerical homogenization technique and has been newly introduced to simulate the mechanical behaviour of composites with randomly distributed inclusions. The volume fraction of the inclusions is the first main parameter in the model. To take the matricity as a further microstructural parameter into account, the self-consistent embedded cell model has been extended by a second self-consistent embedded cell model, Fig. 2. In this "matricity model", we are able to define the matricity in the same manner as it is defined for a real microstructure: first, the single phases are reduced to skeleton lines S_α and S_β by shrinking each phase to a single line, [starting from interfaces] and using standard image analyses procedures, [20]. Then, matricity M_i of a phase i ($i = \alpha, \beta$) is defined as the normalised skeleton line length $M_\alpha = S_\alpha/(S_\alpha + S_\beta)$ and $M_\beta = S_\beta/(S_\alpha + S_\beta)$ with $M_\alpha + M_\beta = 1$. The lengths of the skeleton lines of the inclusions (Fig. 2; left: β, right: α) are zero as the inclusions are perfectly spherical and are, therefore, reduced to a point in the process of obtaining the matricity of the phase.

The lengths of the skeleton lines S_α and S_β in the matrices are given as the circumference of a circle with a diameter which is obtained from the arithmetic average of the diameter of the embedded cell and the diameter of the inclusion phase (Fig. 2; left: S_α, right: S_β). The diameters of the embedded cells are denominated as W_1 and W_2. The diameters of the inclusion part of the embedded cells depend on the volume fraction of the inclusions and the corresponding factors W_1 or W_2. The matricity M can be calculated as a function of the sizes of the embedded cells and the volume fraction of one of the two phases, and the volume fraction of the phases is held constant in both parts of the matricity model.

As can be seen in Fig. 2, the volume fractions and, thus, the diameters W_1 and W_2 of the embedded cells are adjustable. To achieve a matricity value M_i ($i = \alpha, \beta$) as obtained in the experiments, the measured volume fraction of the phases in the model is realized, and the diameters W_1 and W_2 are calculated according to [15],

$$
\begin{aligned}
W_1 &= W_2\left(\sqrt[3]{1-f_\beta}+1\right)\frac{1-M_\beta}{M_\beta\left(\sqrt[3]{f_\beta}+1\right)}, \quad W_2 = 1 \text{ for } M_\beta \geq 0,5, \\
W_2 &= W_1\left(\sqrt[3]{1-f_\alpha}+1\right)\frac{1-M_\alpha}{M_\alpha\left(\sqrt[3]{f_\alpha}+1\right)}, \quad W_1 = 1 \text{ for } M_\alpha \geq 0,5 \ .
\end{aligned}
\tag{1}
$$

If the geometrical boundary conditions are modelled at a distance of about five times the radius of the embedded cell, they are of almost no influence on the model's mechanical behaviour; the continuum mechanical stress-stain state in the embedded cell is hardly influenced as well. Due to the virtual independency from remote boundaries, it is not necessary to model the matricity as an absolute parameter of the FE mesh. Rather, it is possible to introduce the matricity by adjusting the weighting factors W_1 and W_2 only in the evaluation of the results from the inclusion type geometries. As the stresses and strains of the model have to be determined by an iterative procedure in about three to five iterations, the adjusting weighting factors W_1 and W_2 must be introduced in the evaluation of each iteration step.

In principle, stress-strain curves of the two-phase composite are determined from the matricity model in the same iterative manner as it is done for the simple self-consistent embedded

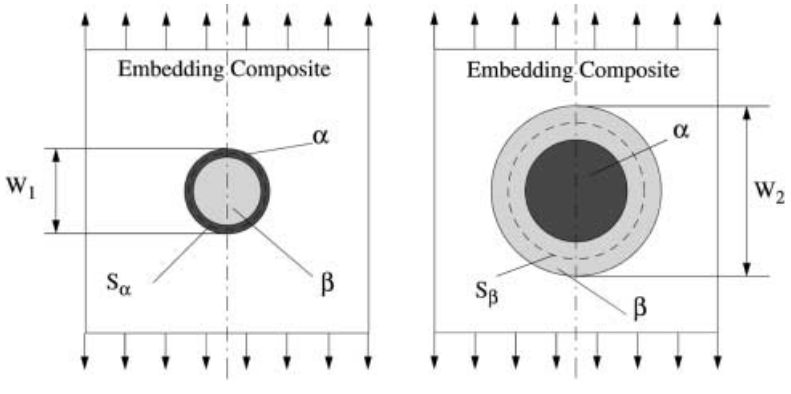

Fig. 2. Matricity model (schematic) consisting of two parts with skeleton lines to adjust for the measured parameter of matricity in the 2D or 3D (axisymmetric) model via the factors W_1 and W_2

cell model, [8, 9]: in each increment of the iteration, the components for stress and strain are determined. This is done by a weighted averaging of all stress and strain values over all integration points of both embedded cells.

Interpenetrating microstructures, where both phases can show percolation throughout the material, are characterized by the above introduced matricity parameter M with values between zero and one, describing the mutual material circumscription of the phases in addition to their volume fractions. The matricity model is based on 2D or 3D (axisymmetric) inclusions of a given volume fraction and with circular cross section in the present context, [11–17, 21]. Thus, this model shows the same effect as a single model with two included composites α-β and β-α as in the experiment, cf [14, 15]. In this paper, all calculations were performed with the 3D (axisymmetric) version of the model.

The model in Fig. 2 allows for additional consideration of thermal residual stresses and can be used to predict the elastic properties, the thermal expansion coefficient and the elastic-plastic stress-strain curves for different phase arrangements as well as to predict phase properties of the phases in the composite. For comparison reasons, the Tuchinskii model is introduced as a second one which allows to predict upper and lower bounds of the elastic modulus E of a composite with interpenetrating microstructures by the following formulae, [22],

$$\frac{E}{E_\alpha} = (1-c)^2 + \left(\frac{E_\beta}{E_\alpha}\right)c^2 + \frac{(E_\beta/E_\alpha)c(1-c)}{c+(E_\beta/E_\alpha)(1-c)} \quad \text{lower bound,}$$
$$\frac{E}{E_\alpha} = \left[\frac{1-c}{(1-c^2)+(E_\beta/E_\alpha)c^2} + \frac{c}{(1-c)^2+(E_\beta/E_\alpha)(2-c)c}\right]^{-1} \quad \text{upper bound ,} \tag{2}$$

where E_i = Young's modulus of phase i, f_i = volume fraction of phase i ($i = \alpha, \beta$) while $f_\beta = (3–2c)c^2$ is the relation between the volume fraction f and the geometry parameter c (real solution between 0 and 1).

In a third model by Pompe, the calculation of the thermo-elastic constants is also based on the solution of an inclusion problem, [23]. Due to the ellipsoidal shape of the inclusions, the fields inside the inclusions are homogeneous and can be determined analytically. Throughout this paper, we assume the special case of spherical inclusions. Interaction between the media can be considered through assumptions about the surrounding material. This is often realized by the effective medium theory (EMA). For the mean stress and strain fields, self-consistency is claimed leading to an implicit equation system which allows for the determination of the effective constants. The effective values for Young's modulus, thermal expansion coefficient, [14], as well as residual stresses, [24], are then determined numerically.

3
Results and discussion

3.1
Microscopic results

The matricity character M of ZrO_2 has been measured and found to deviate up to 25% from a linear 1:1-relationship, especially at intermediate volume fractions. This result means that ZrO_2 typically represents rather the matrix than an inclusion. Except when the influence of M was investigated, $f = M$ was, therefore, employed for all values of f, Fig. 3.

The thermal expansion coefficient, obtained using the matricity and Pompe models, was determined to behave nonlinearly in a similar manner and to decrease with increasing volume fraction of ZrO_2, Fig. 4.

It is interesting to note that the thermal expansion coefficient is nearly independent on the matricity parameter M, Fig. 5.

Furthermore, the elastic modulus was obtained from the Tuchinski's, Pompe's and matricity models. Upper and lower bounds of the Tuchinski's model as well as that of Pompe were in close agreement to the matricity model. However, the experimental values were scattered in a wide range and, therefore, only partly a good agreement between experiment and simulation was achieved, Fig. 6. Residual stresses are not considered in the models used to calculate the Young's modulus. When residual stresses are taken into account, the stress-strain curve of the composite calculated by the matricity model does not frequently show an initial elastic behaviour.

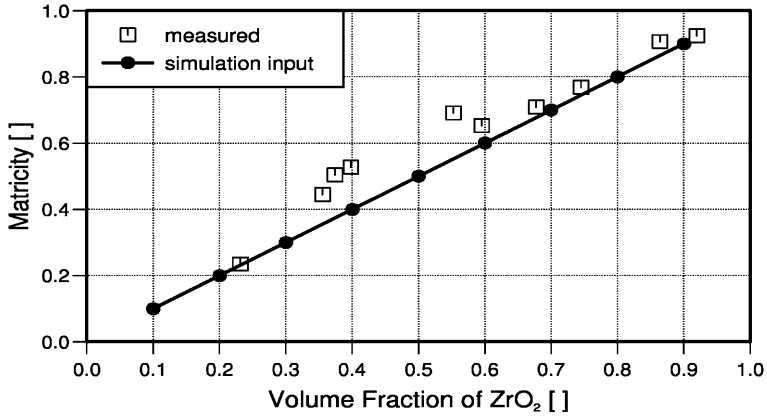

Fig. 3. Matricity of ZrO_2 vs. volume fraction of ceramic (ZrO_2) in ZrO_2/NiCr 80 20 composite

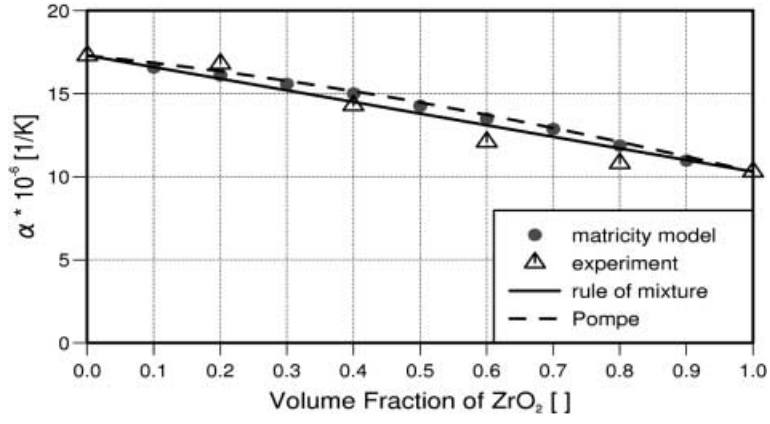

Fig. 4. Thermal expansion coefficient vs. volume fraction of ceramic (ZrO_2). Comparison between experiment, matricity model, rule of mixture and Pompe model, [23]

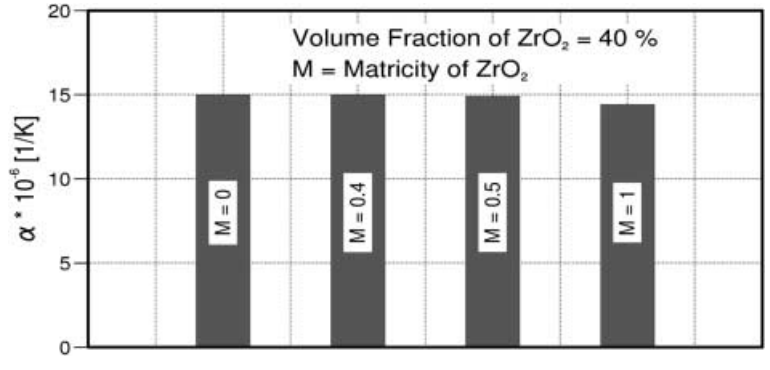

Fig. 5. Thermal expansion coefficient as a function of matricity parameter $M = M_{ZrO_2}$. Volume fraction of ceramic $f_{ZrO_2} = 40\%$

In Fig. 7, the influence of the volume fraction of ZrO_2 on the stress-strain curves of ZrO_2/NiCr 80 20 composites is studied. Strong variations in the plastic behaviour are found especially for $f_{ZrO_2} = 30\%–60\%$, the regime of the phase interpenetration. Therefore, this regime of volume fractions is relevant when a variation of the mechanical behaviour of the composite is required without manipulating matricity.

Matricity plays a major role specifically at low ceramic volume fractions, Fig. 8, while residual stresses are of less importance at all volume fractions. From this result it is obvious, that the matricity parameter provides a strong potential for designing the mechanical behaviour of

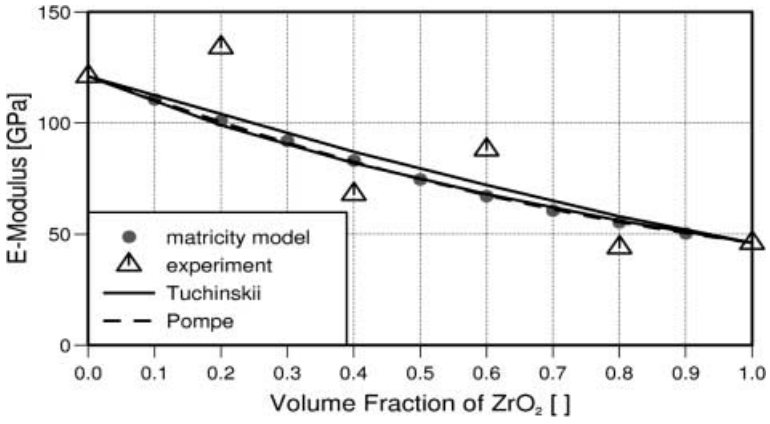

Fig. 6. Elastic modulus vs. volume fraction of ceramic (ZrO_2). Comparison between the matricity model, Tuchinskii model, [22], and Pompe model, [23], (no residual stresses)

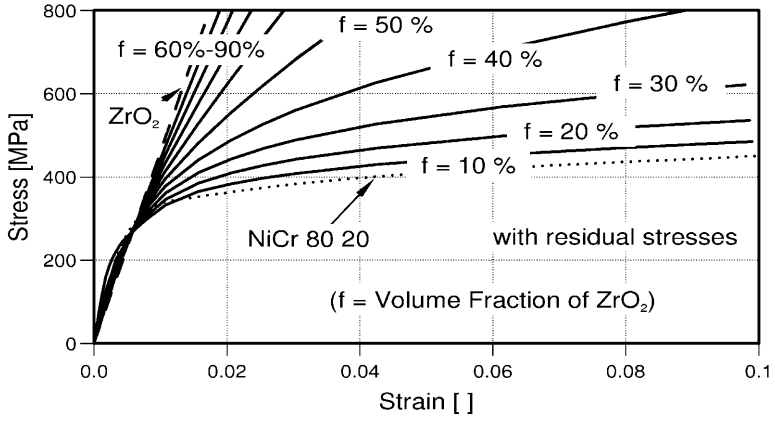

Fig. 7. Stress-strain curves for several volume fractions f_{ZrO_2} of ceramic. Matricity of the ceramic phase (ZrO_2) according to Fig. 3 (with residual stresses)

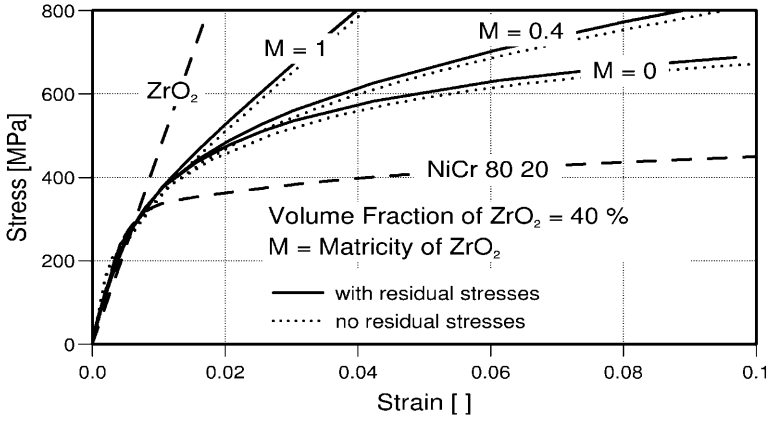

Fig. 8. Stress-strain curves for a volume fraction of ceramic f_{ZrO_2} = 40%. Variation of matricity M_{ZrO_2} (with and without residual stresses)

the composite. On the other hand, residual stresses can be of major importance with respect to failure in the phases.

The ZrO_2 phase depicts typically compressive residual stresses with a sharp peak value, while the NiCr phase depicts tensile residual stresses with a broad, wide distribution. This is mainly due to the fact that, at low volume fractions, ZrO_2 is basically present as a small inclusion, thus following Eshelby's constant stress rule for spherical inclusions, [25], while NiCr, as mainly a

matrix phase, shows a wide variation of stress levels, as expected from inhomogeneous strains in local shear bands around the ZrO_2 inclusions, [9]. The average stresses (circumferential component) in the phases are shifted to higher values at a higher volume fraction of ZrO_2 (Fig. 9) as a result of the increasing influence of the stiffer ceramic.

It is obvious that the stress distributions depict width due to the fact that in one part α surrounds β, and v.v in the other part of the model. This is also the reason for the effect that the stresses in the low volume phase ZrO_2 show two peaks for f_{ZrO_2} = 40% in Fig. 9b.

The agreement between calculations and experiments for the average stress values in either phase is found to be rather good for both phases, Fig. 10, [24]. This fact suggests the effectiveness of the matricity model as a new homogenization procedure. It's superiority in predicting local surface properties has been demonstrated recently for metal/metal composites, [15].

3.2
Macroscopic Results

The knowledge of the mechanical properties of ZrO_2/NiCr 80 20 composites can be used by applying it to simulate FGM. The dependence of the macroscopic behaviour of a graded metal/

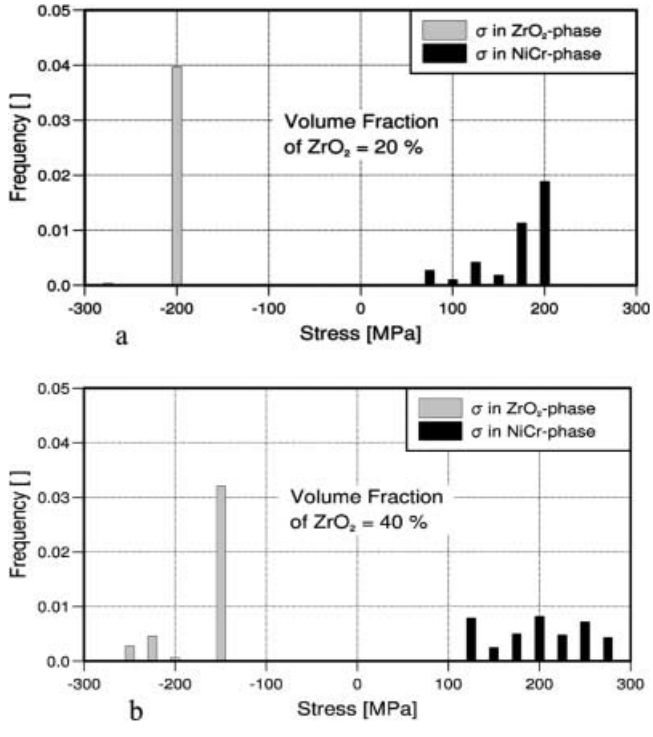

Fig. 9. Calculated distribution of circumferential residual stresses obtained with the matricity model in the ceramic (ZrO_2) and metal phase (NiCr) for a volume fraction of ceramic **a** f_{ZrO_2} = 20% and **b** f_{ZrO_2} = 40%

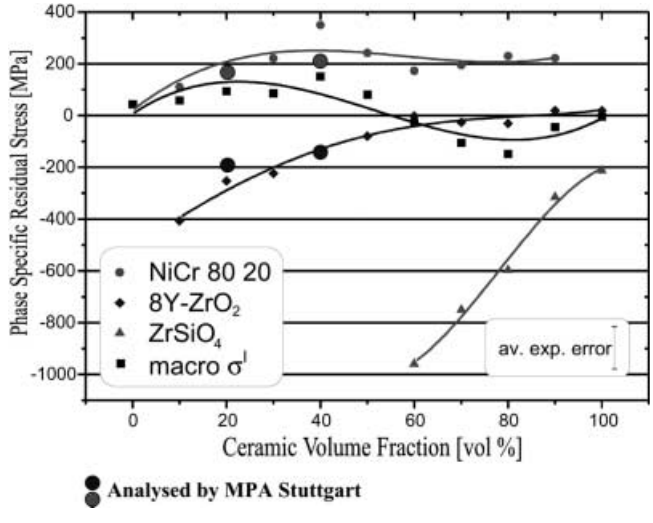

Fig. 10. Experimentally measured, [24], and numerically (matricity model) analysed residual stresses in a ZrO_2/NiCr 80 20 composite at several phase compositions

ceramic composite can be derived by taking the local material behaviour into account. In the present context, locally different microstructural compositions, and thus different material properties, are considered by a layered model with different material properties in each layer. As a model, a bending specimen is chosen, where the transition from the ceramic to the metal phase was realised by four layers (FGM specimen) as well as by a sharp interface (nongraded specimen). The FE mesh, boundary conditions as well as layer subdivision of ungraded and graded specimen are shown in Fig. 11. For the FGM specimen, the matricities (and according to

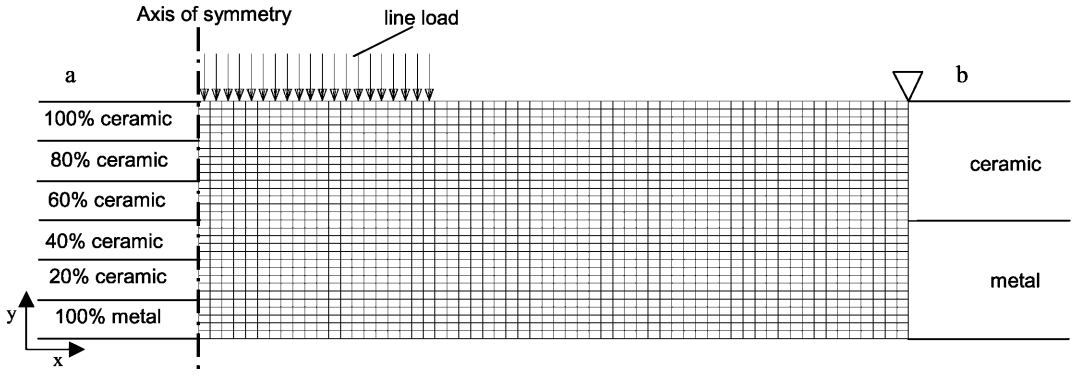

Fig. 11. Graded **a** and non-graded **b** bending specimen

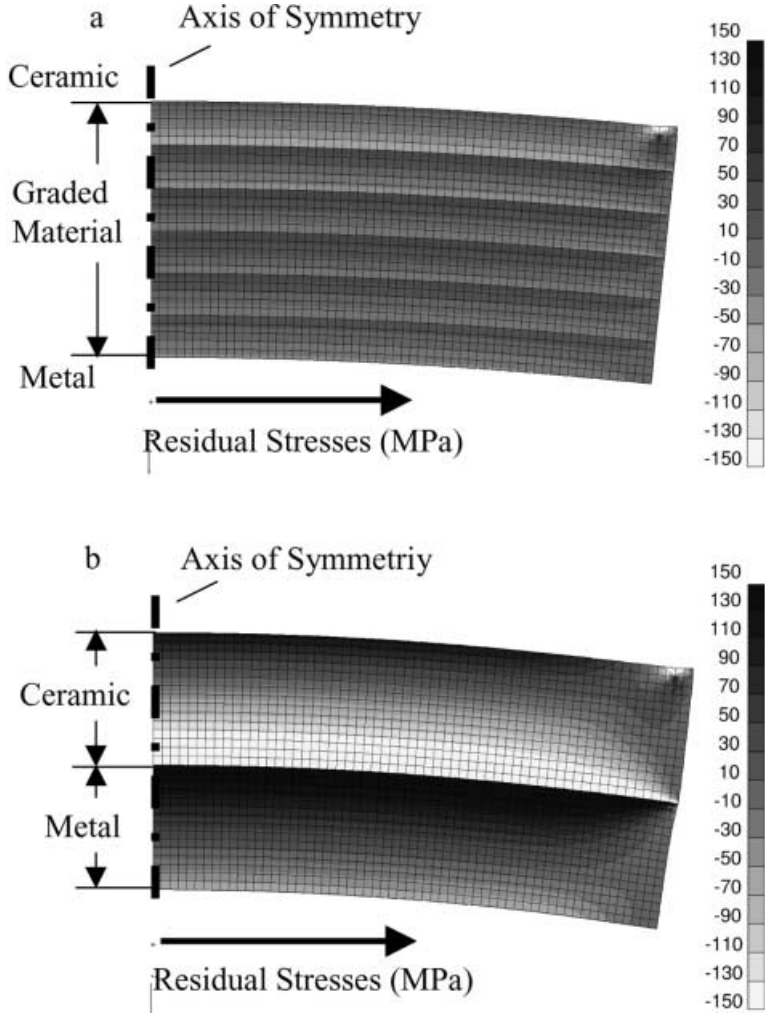

Fig. 12. Distribution of residual stresses in a graded **a** and in a non-graded **b** specimen after cooling down by −750 K; stresses parallel to the layers

Sec. 3.1, therefore, its properties) are varied from layer to layer, besides the volume fractions. In addition to the measured matricity value M ($M \sim f$, Fig. 3), three different matricities $M = 0$, $M = 0.5$ and $M = 1$ were assumed in the layers containing 20%–80% ceramic phase. In the present context, $M = M_{ZrO_2}$, thus $M = 1$ defines an inclusion phase with ceramic matrix. In the first step, the specimen is cooled down from an assumed stress-free state by 750 K, in order to simulate the manufacturing process of the specimen. In Fig. 12, the residual stresses parallel to the layers are shown as fringe plots. As expected, the graded specimen (Fig. 12a) shows significantly smaller residual stresses compared to the nongraded specimen (Fig. 12b). A further reduction of residual stresses parallel to the layers can be expected from even more gradual property transitions in the graded region.

However, the distribution of stresses perpendicular to the layers inside the specimen are hardly influenced by the composition of the specimen, while the nongraded composite shows stronger disturbances of the stresses at the free edge, Fig. 13. In the second step, the specimen is heated up to 500 °C and then loaded by an area load of 600 N/mm^2 corresponding to a resultant force of 24 kN. By this, the behaviour of the specimen is simulated under thermal-mechanical loading. Figure 14 shows the macroscopic force-displacement behaviour of the graded and ungraded bending specimen. It is found that the macroscopic behaviour of the bending specimen can be significantly influenced by the matricity character of the single layers. The larger M_{ZrO_2}, and, therefore, the more metallic phase is circumvented by ceramic phase, the higher the stiffness of the bending specimen. Interestingly, the ungraded metal/ceramic bending specimen shows a similar macroscopic stiffness as compared to the graded specimen with measured matricities, although the stress jumps at the layer interfaces are much smaller in

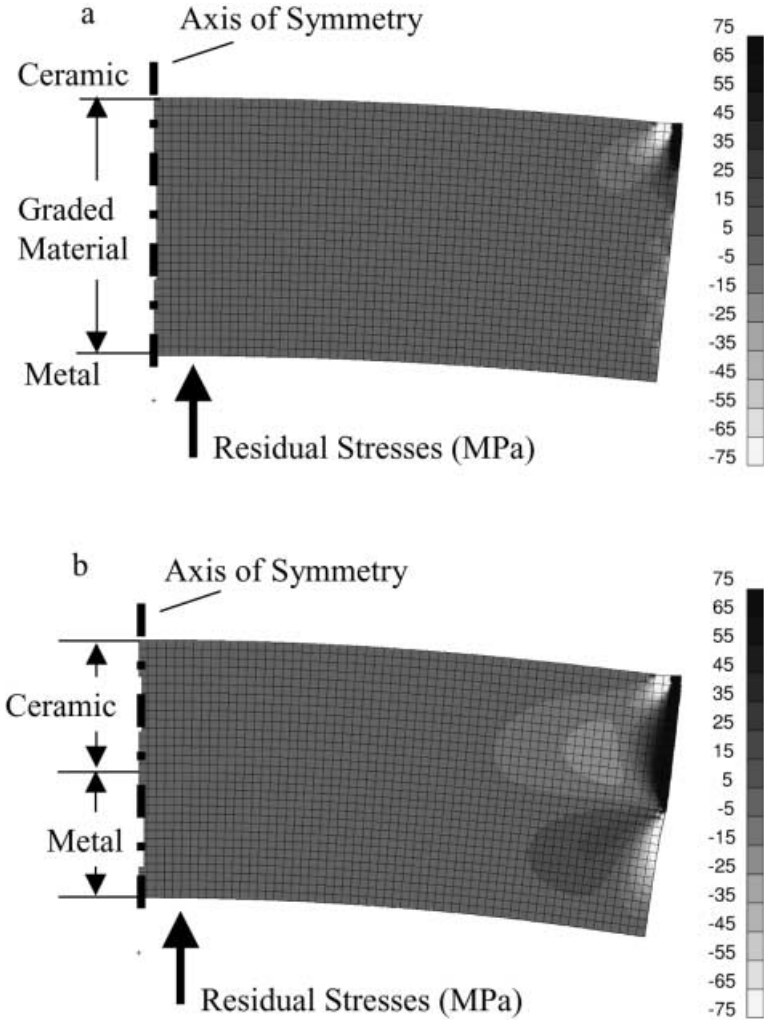

Fig. 13. Distribution of residual stresses in a graded **a** and in a non-graded **b** specimen after cooling down by −750 K; stresses perpendicular to the layers

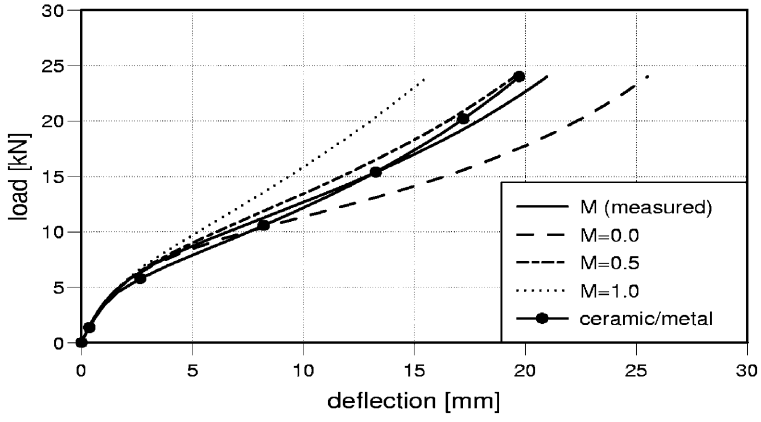

Fig. 14. Deflection behaviour of a graded and a non-graded (ceramic/metal) specimen; influence of the matricity M_{ZrO_2}

the FGM material. Generally, the macroscopic mechanical behaviour of the bending specimen is strongly influenced by the matricity parameter.

4 Conclusions

While the numerical self-consistent embedding cell technique allows to take into account microstructures with randomly arranged inclusions, the matricity model is a sophisticated improved homogenization technique which allows for modelling interpenetrating microstructures. This allows for designing microstructures as well as graded composites, while the proof for manufacturing these microstructure is still to be brought.

References

1. **Dao, M.; Gu, P.; Maewal, A.; Asaro, R. J.:** A micromechanical study of residual stresses in functionally graded materials. Acta Mat 45 (1997) 3265–3276
2. **Noda, N.; Nakai, S.; Tsuji, T.:** Thermal stresses in functionally graded material of particle-reinforced composite. JSME Int JA 41 (1998) 178–184
3. **Reiter, T.; Dvorak, G. J.:** Micromechanical models for graded composite materials: II. Thermomechanical loading. J Mech Phys Solids 46 (1998) 1655–1673
4. **Shen, Y. L.:** Thermal expansion of metal-ceramic composites: A three-dimensional analysis. Mat Sci and En A252 (1998) 269–275
5. **Weissenbek, E.; Pettermann, H. E.; Suresh, S.:** Elasto-plastic deformation of compositionally graded metal-ceramic composites. Acta Mat 45 (1997) 3401–3417
6. **Williamson, R. L.; Rabin, B. H.; Drake, J. T.:** Finite element analysis of thermal residual stresses at graded ceramic-metal interfaces. Part I. Model Description and Geometrical Effects. J Appl Phys 74 (1993) 1310–1320
7. **Zahl, D. B.; Schmauder, S.; McMeeking, R. M.:** Transverse strength of metal matrix composites reinforced with strongly bonded continuous fibers in regular arrangements. Acta Met Mat 42 (1994) 2983–2997
8. **Dong, M.; Schmauder, S.:** Modeling of metal matrix composites by a self-consistent embedded cell model. Acta Met Mat 44 (1996) 2465–2478
9. **Dong, M.; Schmauder, S.:** Transverse mechanical behaviour of fiber reinforced composites – FE modelling with embedded cell models. Comput Mat Sci 5 (1996) 53–66
10. **Schmauder, S.; Dong, M.:** Vorhersage der Festigkeit von Verbundwerkstoffen. Spektrum der Wissenschaft 11 (1996) 18–24
11. **Leßle, P.; Dong, M.; Soppa, E.; Schmauder, S.:** Selbstkonsistente Matrizitätsmodelle zur Simulation des mechanischen Verhaltens von Verbundwerkstoffen. Vortragstexte der Tagung Verbundwerkstoffe und Werstoffverbunde. Kaiserslautern, Hrsg.: K. Friedrich, DGM-Informationsgesellschaft Verlag, Oberursl, September 1997 (1997) 765–770
12. **Schmauder, S.; Dong, M.; Leßle, P.:** Verbundwerkstoffe mikromechanisch simuliert. Metall 7–8/97 (1997) 404–410
13. **Schmauder, S.; Dong, M.; Leßle, P.:** Simulation von Verbundwerkstoffen mit Teilchen und Fasern. XXIV. FEM-Kongreß in Baden-Baden, 17.–18. November 1997, Tagungsband, Hrsg.: A. Streckhardt, Kongreßorganisation, Ennigerloh (1997) 445–462
14. **Leßle, P.; Dong, M.; Schmauder, S.:** Self consistent matricity model to simulate the mechanical behaviour of interpenetrating microstructures. Comput Mat Sci 15 (1999) 455–465
15. **Leßle, P.; Dong, M.; Soppa, E.; Schmauder, S.:** Simulation of interpenetrating microstructures by self consistent matricity models. Scripta Mat 38 (1998) 1327–1332
16. **Schmauder, S.; Weber, U.:** Modelling the deformation behaviour of W/Cu composites by a self-consistent matricity model. ECM'99, Progress in Experimental and Computational Mechanics in

Engineering and Materials Behaviour, 12.–15. September, Urumqi, China, Eds.: Zhu, D.; Kikuchi, M.; Shen, Y.; Geni, M.; Northwestern Polytechnical University Press, Xi'an, China, (1999) 54–60
17. **Dong, M.; Leßle, P.; Weber, U.; Schmauder, S.:** Mesomechanical modelling of composites containing FGM related interpenetrating microstructures based on micromechanical matricity models. Materials Science Forum 308–311. Functionally Graded Materials 1998 (1999) pp. 1000–1005
18. **Jedamzik, R.; Neubrand, A.; Rödel, J.:** Electrochemical processing and characterisation of graded Tungsten/Copper composites. In: Proceedings of the 15th International Plansee Seminar, Vol. 1, Kneringer, G.; Rödhammer, P.; Wilhartitz, P. (eds.) Metallwerk Plansee, Reutte (1997) 1–15
19. **Sautter, M.:** Modellierung des Verformungsverhaltens mehrphasiger Werkstoffe mit der Methode der Finiten Elemente. Diss Universität Stuttgart (1995)
20. **Poech, M.-H.; Ruhr, D.:** Prakt Met Sonderbd 24 (1993) 385–391
21. Abschlußbericht zum DFG-Forschungsvorhaben "Mikro/Mesomechanische Modellierung des mechanischen Verhaltens von Metall/Keramik-Gradientenwerkstoffen" im SPP Gradientenwerkstoffe under contract Schm 746/12-1 and Schm 746/12–2
22. **Tuchinskii, L. I.:** Poroshk Met 7 (1983) 85
23. **Kreher, W.; Pompe, W.:** Internal stresses in heterogeneous solids. Berlin, Akademie-Verlag, 1989
24. **Dantz, D.; Genzel, Ch.; Reimers, W.; Weber, U.; Schmauder, S.:** "Analyse von Makro- und Mikroeigenspannungen in Gradientenwerkstoffen (FGM)", Vortragstexte der Tagung Verbundwerkstoffe und Werkstoffverbunde. Hamburg, Hrsg.: K. Schulte und K.U. Kainer, DGM Informationsgesellschaft Verlag, Weinheim, Oktober 1998, (1998) 704–709
25. **Mura, T.:** Micromechanics of defects in solids. Sec Rev Ed. Dordrecht, The Netherlands, Kluwer Academic Publishers, 1987